



**HAL**  
open science

# Impact of Sputtered AZO Seed Layer Thickness on Hydrothermally Grown ZnO Nanowires Properties for Flexible Perovskite Solar Cells

Karthick Sekar, Johann Bouclé, Raphaël Doineau, Souhir Azzaz, Bruno Schmaltz, Guylaine Poulin-vittrant

## ► To cite this version:

Karthick Sekar, Johann Bouclé, Raphaël Doineau, Souhir Azzaz, Bruno Schmaltz, et al.. Impact of Sputtered AZO Seed Layer Thickness on Hydrothermally Grown ZnO Nanowires Properties for Flexible Perovskite Solar Cells. *Advanced Engineering Materials*, 2025, 10.1002/adem.202401356 . hal-04897648

HAL Id: hal-04897648

<https://unilim.hal.science/hal-04897648v1>

Submitted on 20 Jan 2025

**HAL** is a multi-disciplinary open access archive for the deposit and dissemination of scientific research documents, whether they are published or not. The documents may come from teaching and research institutions in France or abroad, or from public or private research centers.

L'archive ouverte pluridisciplinaire **HAL**, est destinée au dépôt et à la diffusion de documents scientifiques de niveau recherche, publiés ou non, émanant des établissements d'enseignement et de recherche français ou étrangers, des laboratoires publics ou privés.



Distributed under a Creative Commons Attribution 4.0 International License

# Impact of Sputtered AZO Seed Layer Thickness on Hydrothermally Grown ZnO Nanowires Properties for Flexible Perovskite Solar Cells

Karthick Sekar,\* Johann Bouclé, Raphaël Doineau, Souhir Azzaz, Bruno Schmaltz, and Guylaine Poulin-Vittrant\*

Understanding the impact of the aluminum zinc oxide (AZO) seed layer thickness on zinc oxide nanowires (ZnO NWs) growth is decisive in attaining high-quality NWs with higher transparency and without cracking issues when using flexible substrates, especially for optoelectronic applications. Therefore, herein, ZnO NWs have been grown on various thicknesses of AZO films deposited onto flexible substrates (PET, PET/ITO ( $60 \Omega \text{ sq}^{-1}$ ) and ( $200 \Omega \text{ sq}^{-1}$ )) through a simple, low-temperature hydrothermal growth process. Based on AZO layer thickness, structural, optical, morphological, and topographical properties have been systematically investigated. The results demonstrate that 1) thicker AZO films ( $\approx 250 \text{ nm}$ ) increase the crystallinity of the ZnO NWs than thinner AZO films ( $\approx 200$  and  $100 \text{ nm}$ ). 2) ZnO NWs on the thicker AZO films with different ITO grades ( $60$  or  $200 \Omega \text{ sq}^{-1}$ ) provide an optical bandgap value of  $3.24\text{--}3.27 \text{ eV}$  and offer good transmittance ( $>80\%$ ) in the visible range. 3) The AZO film thickness strongly influences ZnO NWs growth, especially NWs' average diameter and density. 4) Annealing the samples at  $100^\circ \text{C}$  after NW growth is pointless. Overall, the findings demonstrate efficient tuning of the ZnO NW properties that exhibit promising potentiality for perovskite solar cells, which have also been preliminarily tested.

photocatalysts,<sup>[10]</sup> and so on. These applications are enabled by their adjustable physical properties, such as wide bandgap ( $3.37 \text{ eV}$ ),<sup>[11]</sup> high electron mobility ( $200\text{--}300 \text{ cm}^2 \text{ Vs}^{-1}$ ),<sup>[12]</sup> high exciton binding energy ( $60 \text{ meV}$ ),<sup>[13]</sup> and high conductivity.<sup>[14]</sup> So far, various physical and chemical methods have been considered to synthesize ZnO NWs, such as hydrothermal growth (HTG) and/or chemical bath deposition (CBD),<sup>[15,16]</sup> vapor-liquid-solid process,<sup>[17]</sup> flame transport approach,<sup>[18]</sup> pulsed laser deposition,<sup>[19]</sup> molecular beam epitaxy,<sup>[20]</sup> and electrospinning.<sup>[21]</sup> However, low-temperature HTG is the most promising technique for growing ZnO NWs over flexible substrates such as polyethylene terephthalate (PET).<sup>[22,23]</sup> Indeed, other synthesis methods usually require high temperatures, which will damage the flexible substrates.<sup>[24]</sup> Moreover, the HTG process offers several advantages like low cost, environmentally friendly, and easy processing.

In SCs, especially in flexible perovskite SCs (FPSCs), ZnO NWs have been used as an alternative electron transport layer (ETL) instead of conventional  $\text{TiO}_2$ , which usually needs high-temperature ( $>450^\circ \text{C}$ ) processing.<sup>[25,26]</sup> In addition, it shows excellent bulk electron mobility (for ZnO  $205\text{--}300 \text{ cm}^2 \text{ V}^{-1} \text{ s}^{-1}$  and for  $\text{TiO}_2$   $0.1\text{--}4 \text{ cm}^2 \text{ V}^{-1} \text{ s}^{-1}$ ), high transparency, simple and easy preparation, and better environmental stability than  $\text{TiO}_2$ .<sup>[27,28]</sup> Moreover, due to their fewer

## 1. Introduction

Zinc oxide (ZnO) nanostructures, especially nanowires (NWs), have gained broad attention and are useful for several practical applications, such as piezoelectric nanogenerators,<sup>[1]</sup> solar cells (SCs),<sup>[2,3]</sup> light-emitting diodes,<sup>[4]</sup> lasers,<sup>[5]</sup> gas and biological sensors,<sup>[6,7]</sup> UV photodetectors,<sup>[8]</sup> marine antifouling systems,<sup>[9]</sup>

K. Sekar, R. Doineau, G. Poulin-Vittrant  
GREMAN UMR 7347  
Université de Tours, CNRS, INSA Centre Val de Loire  
37071 Tours, France  
E-mail: karthick.sekar@univ-tours.fr;  
guylaine.poulin-vittrant@univ-tours.fr

 The ORCID identification number(s) for the author(s) of this article can be found under <https://doi.org/10.1002/adem.202401356>.

© 2025 The Author(s). Advanced Engineering Materials published by Wiley-VCH GmbH. This is an open access article under the terms of the Creative Commons Attribution License, which permits use, distribution and reproduction in any medium, provided the original work is properly cited.

DOI: 10.1002/adem.202401356

K. Sekar, J. Bouclé, S. Azzaz  
Univ. Limoges, CNRS, XLIM, UMR 7252  
F-87000 Limoges, France

S. Azzaz  
Group of Organic Electronic and Molecular Photovoltaic Devices  
Laboratory of Condensed Matter and Nanosciences  
Faculty of Sciences of Monastir  
University of Monastir  
5019 Monastir, Tunisia

B. Schmaltz  
PCM2E EA 6299  
Université de Tours  
Parc de Grandmont, 37200 Tours, France

grain boundaries and defects, vertically growing ZnO NWs efficiently transport the electrons from the light absorber to the bottom electrode, such as indium tin oxide (ITO)-coated PET.<sup>[29,30]</sup> In 2013, the first report based on ZnO nanorods ETL (i.e., grown by CBD) consisted of FPSCs with a device structure of PET/ITO/ZnO NRs/MAPbI<sub>3</sub>/spiro-OMeTAD/Au, offering a power conversion efficiency (PCE) of 2.6%.<sup>[31]</sup> The authors prove that ZnO NRs-based FPSC offers better charge collection and heterojunction interface than a conventional rigid SC. Later, in 2016, Dymshits et al. investigated and published a ZnO NWs-based FPSC (PET/ITO/ZnAc/ZnO NW/MAPbI<sub>3</sub>/Spiro-OMeTAD/Au) showing PCE of 6.3%, and the device demonstrated good stability even after 75 bending cycles.<sup>[32]</sup> Recently published reports from Sun et al. (2019)<sup>[33]</sup> and Fahim et al. (2021)<sup>[34]</sup> show that achieving almost 9 and 13% of efficiency is possible using ZnO NWs ETL in FPSCs. Their results revealed that the applied external tensile strain over the SC significantly enhances the photovoltaic performance compared to the compressive strains. Noticeably, positive piezoelectric potential is generated at the perovskite absorber/ZnO NWs interface by a tensile strain that reduces the charge transfer barrier height and enhances the electron transport from the absorber to ZnO NWs and then to the corresponding electrode. Conversely, compressive strains induce the negative piezoelectric potential and increase charge barrier height, affecting charge transport that reduces the performance.<sup>[33,34]</sup> Therefore, the understanding of the influence of each layer on the SC performance is essential to further improve the efficiency of devices based on ZnO NWs. For example, seed layers such as ZnO and aluminum-doped ZnO (AZO), as well as their thickness, are crucial to achieving high-quality ZnO NWs.<sup>[1,35]</sup> As a consequence, optimizing the seed layer thickness is highly essential, and of course, it also depends on the substrates (either rigid/flexible) and the fabrication strategies, etc. As far as we know, up to date, there are countable reports only available using ZnO NW ETL-based FPSCs.<sup>[11–16]</sup> More importantly, in all these flexible device reports, the researchers used the ZnO seed layer, and interestingly, in our work, we have adopted the AZO seed layer, which is completely novel. For more information, check our recently published review on the control of ZnO NWs growth in FPSCs.<sup>[36]</sup> Rezaie et al. report that the growth orientation is better, and the growth rate of the ZnO NWs on the AZO seed layer along the [0001] direction is faster than on a ZnO seed layer.<sup>[37]</sup> The AZO seed layer's improved structural and morphological properties offer better and uniform ZnO NWs growth than the ZnO seed layer.<sup>[38]</sup> In particular, Nirmal Peiris et al. explain that the compact nature and the thickness of the sputtered seed layer (ZnO or AZO) are crucial to achieving uniform and well-aligned ZnO NWs growth on flexible substrates.<sup>[39]</sup>

Furthermore, Dehghan Nayeri et al. showed that the ZnO NWs grown on the AZO seed layer film displayed an improved optical behavior compared to the ZnO seed layer film.<sup>[40]</sup> Matheson et al.'s reports demonstrate that the ZnO NWs growth on the AZO nanoparticle seed layer film offers high-quality uniform ZnO NWs with enhanced optical properties for optoelectronic applications.<sup>[41]</sup> Hrilina Ghosh et al.'s study evidences the effect of different levels of Al-incorporated ZnO NW growth on the AZO seed layer compared to the conventional ZnO NWs, resulting in considerable improvement in the near-band-edge

ultraviolet emission and the optical bandgap values.<sup>[42]</sup> Quang Chieu Bui et al. demonstrated the AZO thin-film deposition by atomic layer deposition (ALD) process, followed by the ZnO NW growth by the pulsed liquid injection metal–organic chemical vapor deposition process. Mainly, they varied the Al dopant concentrations of AZO films by adjusting the Zn/Al precursor cycle ratio in the ALD process, which influenced the structural orientations of the deposited AZO thin films and subsequently impacted the growth direction of ZnO NWs.<sup>[43]</sup> Moreover, Serrano et al. systematically studied the influence of the AZO seed layer deposition method, such as ultrasonic spray pyrolysis (USP) and magnetron sputtering, confirming that the seed layer deposition method has a significant impact on the structural, morphological, and optical properties of the deposited AZO layer and subsequently on the ZnO NWs growth and their properties.<sup>[44]</sup> In addition, Wan Shu Cheng et al. reported that extreme bending of the flexible substrates significantly cracks the AZO seed layer, which causes severe damage to the fabricated device performance and leads to failure (i.e., nonworking devices), even if the tested film is returned to its original state.<sup>[45]</sup> Therefore, it is essential to understand the impact of the chosen AZO seed layer thickness to attain high-quality ZnO NWs growth with higher transparency and without cracking issues when using flexible substrates.

Therefore, in this work, ZnO NWs are grown on flexible PET/ITO (60 and 200 Ω sq<sup>-1</sup>)/AZO and pure PET/AZO (i.e., without ITO) substrates by a low-temperature HTG to understand the structural, morphological, optical, and topographical properties, with regard to the photovoltaic application. Different AZO seed layer thicknesses were tested and characterized to demonstrate well-aligned and uniform ZnO NWs, suitable for FPSC fabrication. We especially discuss the impact of AZO layer thickness on the ZnO NWs growth. The following findings are noticed: a thicker AZO layer offers 1) better crystallinity, 2) considerably improved transmittance over 80% in the visible region, 3) the AZO film thickness strongly impacts ZnO NWs growth, especially ZnO NWs' average diameter and density, and 4) annealing the samples after NW growth at 100 °C is unnecessary. Later, the optimized ZnO NWs were grown on flexible substrates tested as an ETL in order to transport (block) the electrons (holes) from the perovskite to the front electrode. Overall, we managed to optimize the ZnO NW growth on flexible substrates to be suitable ETLs for FPSCs, which were then preliminarily tested in this work.

## 2. Experimental Section

### 2.1. Materials

#### 2.1.1. For ZnO NWs

The commercial PET/ITO substrates ((i) product number 639 303 1EA, surface resistivity 60 Ω sq<sup>-1</sup>, (ii) product number 749 745 1EA, surface resistivity 200 Ω sq<sup>-1</sup>) and pure PET substrates (without ITO, product number GF09063581) were purchased from Sigma Aldrich. Zinc nitrate hexahydrate Zn(NO<sub>3</sub>)<sub>2</sub>·6H<sub>2</sub>O (product number 96 482, 98%), hexamethylenetetramine (HMTA) (CH<sub>2</sub>)<sub>6</sub>N<sub>4</sub> (product number 33 233, >99.5%), and polyethylenimine branched (PEI) (number 408 727, average

Mw  $\approx$  25 000) were purchased from Sigma-Aldrich, also used as received.

### 2.1.2. For PSCs

Formamidinium iodide (FAI) (90%, GreatCell Solar, Queanbeyan, Australia), cesium iodide (CsI) (99.9%, trace metals basis, Sigma Aldrich, St. Louis, MO, USA), lead iodide (PbI<sub>2</sub>) (99%, Sigma Aldrich), lead bromide (PbBr<sub>2</sub>) (90%, Sigma Aldrich), Spiro-OMeTAD (99% HPLC, Sigma Aldrich), 4-tert-butylpyridine (96%, Sigma Aldrich), Bis (trifluoromethane) sulfonimide lithium salt (99.95%, Li-TFSI, trace metals basis, Sigma Aldrich), chlorobenzene (CB, anhydrous, 99.8%, Sigma Aldrich), N-N dimethylformamide (DMF, anhydrous, 99.8%, Sigma Aldrich), dimethyl sulfoxide (DMSO anhydrous, 99.9%, Sigma Aldrich), acetonitrile (anhydrous, 99.8%, Sigma Aldrich), and diethyl ether (DEE, 99.5%, GC, Sigma Aldrich) were also used as received.

## 2.2. Procedures for ZnO NWs Growth and PSC Fabrication

### 2.2.1. The ZnO NWs Growth

Clear transparent and fresh stock solutions of Zn(NO<sub>3</sub>)<sub>2</sub> (1.5 g) and HMTA (0.87 g) were separately prepared in 100 mL of deionized water (DI) and a PEI (1.25 g) in 10 mL of DI solution. To hydrothermally grow ZnO NWs, the stainless steel autoclave was filled with the prepared solutions in the following order: Zn(NO<sub>3</sub>)<sub>2</sub> (30 mL), HMTA (30 mL), PEI (1 mL), and DI (39 mL). **Figure 1a** shows the schematic representation of ZnO NW growth setup and procedures. The substrates (pure PET and PET/ITO, 2 × 2 cm<sup>2</sup>) were ultrasonically cleaned using ethanol, isopropanol, and DI water for 10 min before depositing the AZO seed layer. The AZO seed layer was deposited with physical vapor deposition equipment (Plassys MP 550 S) without heating the substrates (65 W, 5 mTorr).<sup>[1]</sup> After that, the AZO-deposited PET and PET/ITO substrates were etched with a DECO084 laser femtosecond equipment. Later, the PET/ITO/AZO and PET/AZO films were carefully placed in the designed sample holder (**Figure 1a**), which was transferred into the stainless steel autoclave to grow ZnO NWs. After hermetically sealing the stainless steel autoclave, the system was heated up to 85 °C for 6 h, including a 30–40 min ramp of temperature, same as our previous report.<sup>[46]</sup> Finally, the substrates were carefully taken outside and cleaned with the DI (especially the backside) before any other layer deposition or characterizations.

For simplicity, PET (without ITO), PET/ITO (60 Ω sq<sup>-1</sup>), and PET/ITO (200 Ω sq<sup>-1</sup>) substrates are hereafter denoted as PET, PET-ITO<sub>60</sub>, and PET-ITO<sub>200</sub>, respectively. Different AZO seed layer thicknesses ( $\approx$ 100,  $\approx$ 200, and  $\approx$ 250 nm) were deposited on PET, PET-ITO<sub>60</sub>, and PET-ITO<sub>200</sub> by radio frequency sputtering. Again, for easiness, different thicknesses of AZO seed layers, such as  $\approx$ 100,  $\approx$ 200, and  $\approx$ 250 nm, are represented as AZO<sub>100</sub>, AZO<sub>200</sub>, and AZO<sub>250</sub>, respectively. In addition, substrates (i.e., PET, PET-ITO<sub>60</sub>, and PET-ITO<sub>200</sub>) with different thicknesses of AZO seed layers (i.e., AZO<sub>100</sub>, AZO<sub>200</sub>, and AZO<sub>250</sub>), especially after ZnO NW growth, were named NW

at the end of the sample name (see **Table 1**). Similarly, the tested annealed (WA) and nonannealed (WOA) PET-ITO<sub>60</sub>-AZO<sub>250</sub>-NW films were indicated as PET-ITO<sub>60</sub>-AZO<sub>250</sub>-NW-WA and PET-ITO<sub>60</sub>-AZO<sub>250</sub>-NW-WOA, respectively.

### 2.2.2. The FPSC Fabrication

Shifting from rigid to flexible substrates usually brings additional challenges in PSC fabrication, especially when using NWs/nanorods as an ETL. For example, Kumar et al.<sup>[31]</sup> and Dumshits et al.<sup>[32]</sup> clearly provide evidence that the flexible devices (PET/ITO/ZnO NR/MAPbI<sub>3</sub>/Spiro-OMeTAD/Au) offer lower efficiencies (2.6%<sup>[31]</sup> and 6.4%<sup>[32]</sup>) compared to the rigid devices (9% for FTO/ZnO NR/MAPbI<sub>3</sub>/Spiro-OMeTAD/Au) due to higher recombination issues at the ZnO NWs/perovskite interface. Also, recent reports<sup>[33,34]</sup> show that achieving over 12% efficiency is possible using ZnO NWs ETL in FPSCs. All the reported ZnO NWs ETL-based FPSCs adopted the n-i-p architecture. Therefore, the same structure (i.e., PET/ITO/AZO/ZnO NWs/FACsPb(Ibr)<sub>3</sub>/hole transport layer [HTL]/Au) was used in our work, as well as the processing method used previously in our group<sup>[2,47,48]</sup> to fabricate the preliminary FPSC devices. It is well-known that the antisolvent treatment enhances the perovskite layer surface morphology<sup>[47–49]</sup> and it is challenging compared to rigid one because the ZnO NW-grown film was not completely flat. Moreover, the spin-coating technique usually requires a vacuum to hold the film, which creates a concave surface in the middle part of the substrate, thus affecting the antisolvent deposition. The schematic representation of FPSC fabrication is shown in **Figure 1b**, similar to our previous publication.<sup>[47]</sup> The prepared perovskite FA<sub>0.85</sub>Cs<sub>0.15</sub>Pb(I<sub>0.85</sub>Br<sub>0.15</sub>)<sub>3</sub>, (simply—FACsPb(Ibr)<sub>3</sub>) solution was spin coated onto the etched ZnO NWs ETL films, including diethyl ether (DEE) antisolvent treatment. After that, the HTL Spiro-OMeTAD, tert-butylpyridine, and Li-TFSI additives, such as reported<sup>[47]</sup> was deposited by spin coating. Finally, the top Au electrode (100 nm) was thermally evaporated through a shadow mask under high vacuum on the HTL layer to complete the device.

## 2.3. Characterizations

The crystal structure of ZnO NWs was examined using X-Ray diffraction (XRD, Bruker AXS D8 discover) operated with CuK $\alpha$  radiation. UV–visible transmittance and absorption spectra were recorded with a Jasco V-670 spectrometer in the wavelength range from 300 to 800 nm. The surface morphology was observed using scanning electron microscopy (SEM, JEOL JSM-7900F). The surface topography was measured with a Dimension ICON Bruker atomic force microscope (AFM, Bruker France SAS, Palaiseau, France). The extraction of the average (avg.) diameters, densities, and RMS values associated with the ZnO NWs were obtained using Image J software on SEM and AFM images. The current density–voltage (*J*–*V*) characteristics of fabricated FPSCs (active area over 0.3 cm<sup>2</sup>) were measured in ambient air without encapsulation using a solar simulator (1600 W NEWPORT) equipped with an AM 1.5G filter and a source meter (Keithley 2400). Device cross-sectional SEM images were recorded using a Zeiss Leo high-resolution microscope.

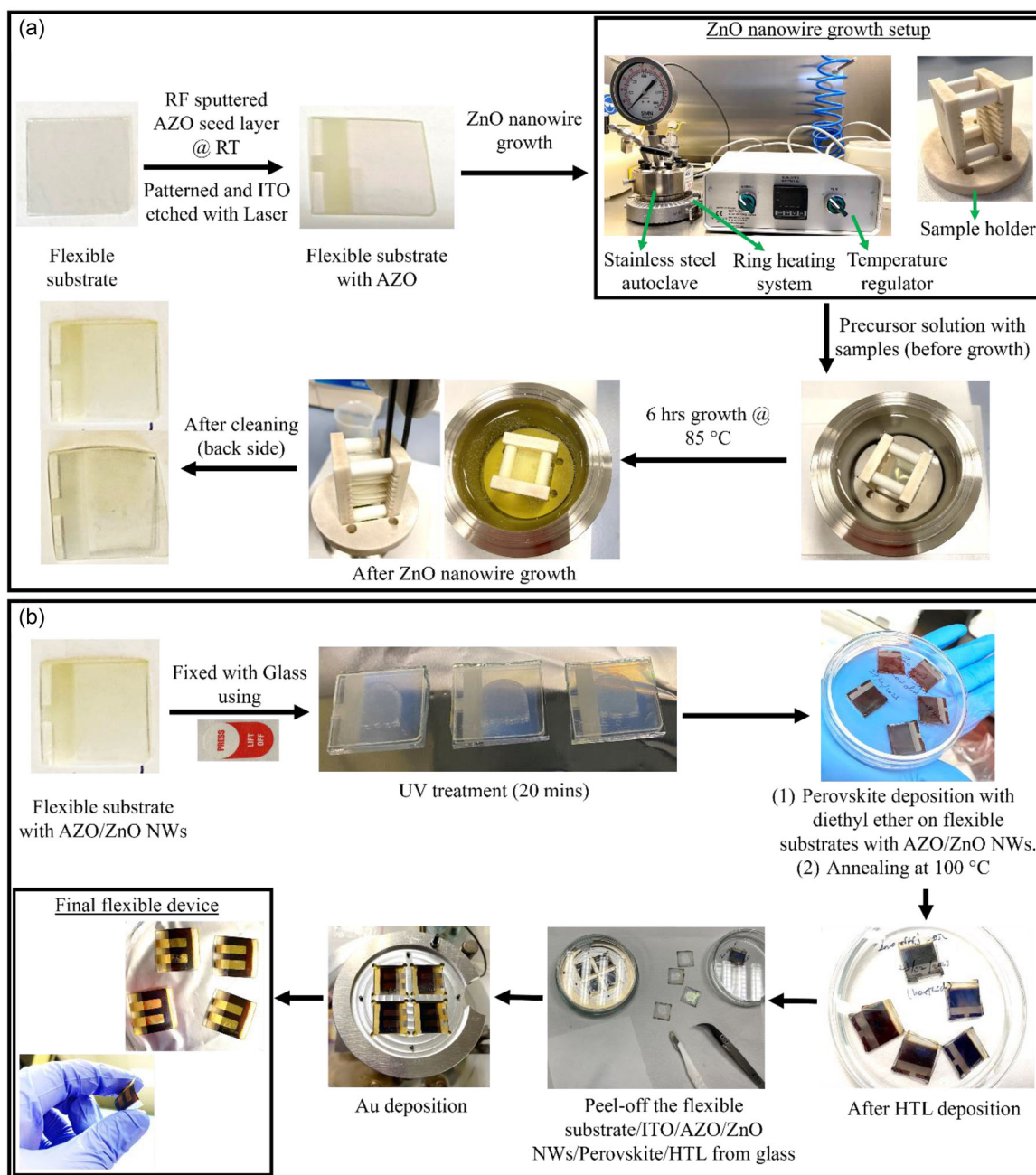


Figure 1. Schematic representation of a) ZnO NWs growth setup and b) PSC fabrication using ZnO NWs on flexible substrates.

### 3. Results and Discussions

The following subsections demonstrate and explain the structural, optical, morphological, and topographical behavior of ZnO NWs on the different flexible substrates (PET-ITO<sub>60</sub>-AZO<sub>100</sub>-NW, PET-ITO<sub>60</sub>-AZO<sub>200</sub>-NW and PET-ITO<sub>60</sub>-AZO<sub>250</sub>-NW, PET-ITO<sub>200</sub>-AZO<sub>100</sub>-NW, PET-ITO<sub>200</sub>-AZO<sub>200</sub>-NW, and PET-ITO<sub>200</sub>-AZO<sub>250</sub>-NW, as well as PET-AZO<sub>100</sub>-NW, PET-AZO<sub>200</sub>-NW, and PET-AZO<sub>250</sub>-NW).

#### 3.1. Structural Analysis

Several reports,<sup>[44,50–53]</sup> including our previously published works,<sup>[1,36,46]</sup> demonstrate that the seed layer thickness strongly influences the ZnO NWs properties, such as length, diameter, density, and aspect ratio. Interestingly, in the study by Serrano et al. ZnO NWs growth on the sputtered AZO seed layer showed a higher (002) orientation with uniform and vertical alignment than USP seed layer-based NWs.<sup>[44]</sup> Indeed, from the

**Table 1.** Sample descriptions for various substrates with AZO layer thickness adopted in this work.

Substrates, AZO layer thickness, NW growth	Stated as
PET (without ITO), 100 nm AZO, Before NW growth	PET_AZO <sub>100</sub>
PET (without ITO), 100 nm AZO, After NW growth	PET_AZO <sub>100</sub> -NW
PET (without ITO), 200 nm AZO, Before NW growth	PET_AZO <sub>200</sub>
PET (without ITO), 200 nm AZO, After NW growth	PET_AZO <sub>200</sub> -NW
PET (without ITO), 250 nm AZO, Before NW growth	PET_AZO <sub>250</sub>
PET (without ITO), 250 nm AZO, After NW growth	PET_AZO <sub>250</sub> -NW
PET/ITO (60 Ω sq <sup>-1</sup> ), 100 nm AZO, Before NW growth	PET-ITO <sub>60</sub> -AZO <sub>100</sub>
PET/ITO (60 Ω sq <sup>-1</sup> ), 100 nm AZO, After NW growth	PET-ITO <sub>60</sub> -AZO <sub>100</sub> -NW
PET/ITO (60 Ω sq <sup>-1</sup> ), 200 nm AZO, Before NW growth	PET-ITO <sub>60</sub> -AZO <sub>200</sub>
PET/ITO (60 Ω sq <sup>-1</sup> ), 200 nm AZO, After NW growth	PET-ITO <sub>60</sub> -AZO <sub>200</sub> -NW
PET/ITO (60 Ω sq <sup>-1</sup> ), 250 nm AZO, Before NW growth	PET-ITO <sub>60</sub> -AZO <sub>250</sub>
PET/ITO (60 Ω sq <sup>-1</sup> ), 250 nm AZO, After NW growth	PET-ITO <sub>60</sub> -AZO <sub>250</sub> -NW
PET/ITO (200 Ω sq <sup>-1</sup> ), 100 nm AZO, Before NW growth	PET-ITO <sub>200</sub> -AZO <sub>100</sub>
PET/ITO (200 Ω sq <sup>-1</sup> ), 100 nm AZO, After NW growth	PET-ITO <sub>200</sub> -AZO <sub>100</sub> -NW
PET/ITO (200 Ω sq <sup>-1</sup> ), 200 nm AZO, Before NW growth	PET-ITO <sub>200</sub> -AZO <sub>200</sub>
PET/ITO (200 Ω sq <sup>-1</sup> ), 200 nm AZO, After NW growth	PET-ITO <sub>200</sub> -AZO <sub>200</sub> -NW
PET/ITO (200 Ω sq <sup>-1</sup> ), 250 nm AZO, Before NW growth	PET-ITO <sub>200</sub> -AZO <sub>250</sub>
PET/ITO (200 Ω sq <sup>-1</sup> ), 250 nm AZO, After NW growth	PET-ITO <sub>200</sub> -AZO <sub>250</sub> -NW
PET/ITO (60 Ω sq <sup>-1</sup> ), 250 nm AZO, After NW growth, with annealing	PET-ITO <sub>60</sub> -AZO <sub>250</sub> -NW_WA
PET/ITO (60 Ω sq <sup>-1</sup> ), 250 nm AZO, After NW growth, without annealing	PET-ITO <sub>60</sub> -AZO <sub>250</sub> -NW_WOA

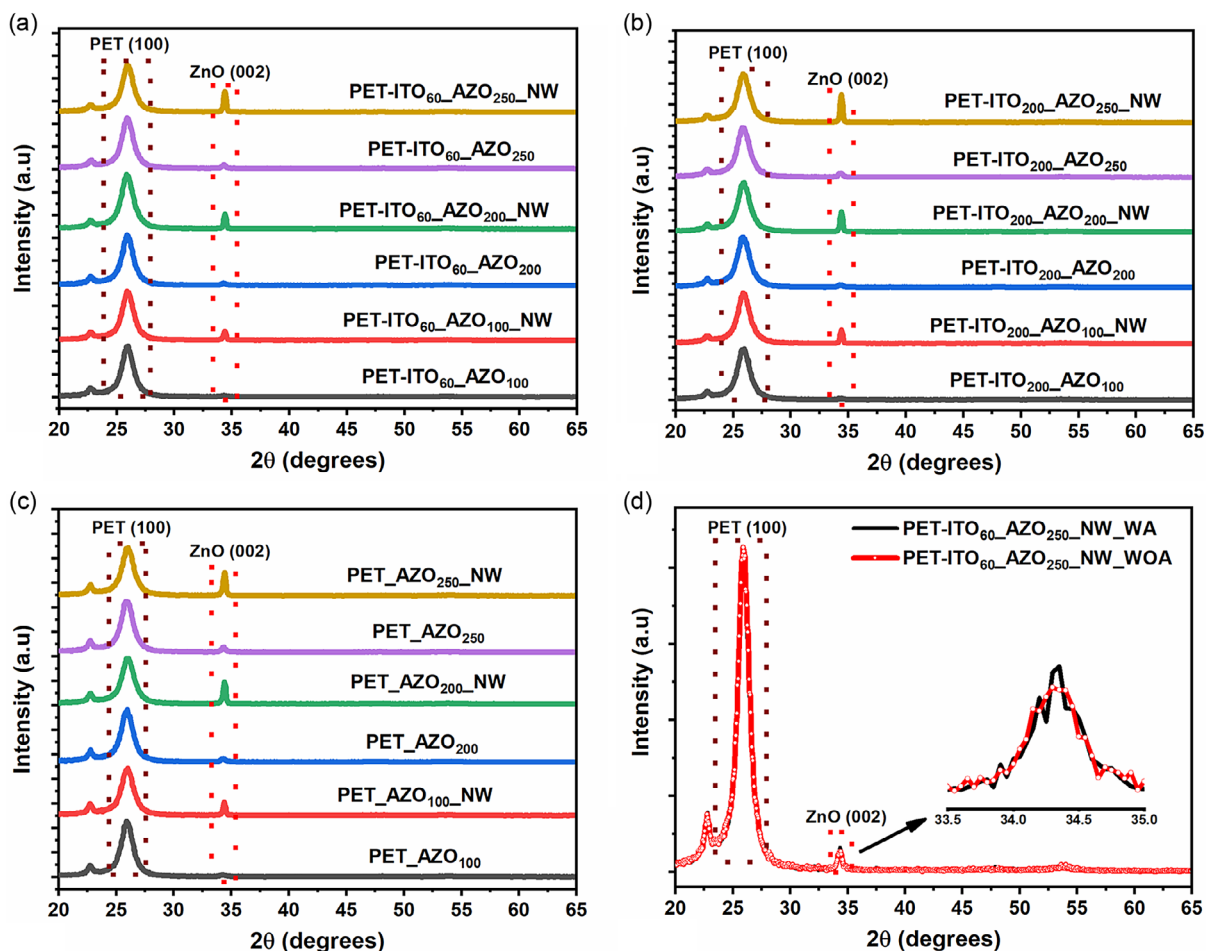
XRD graphs (Figure 2a–c and Figure S1, Supporting Information), especially after ZnO NWs growth, the diffraction peak position at 34.4° corresponding to the c-axis (002) orientation (JCPDS: 36-1451<sup>[54]</sup> and 05-0664<sup>[38]</sup>) is significantly enhanced with an increase in the AZO seed layer thickness. Notably, the highly intense diffraction peak was noticed around ≈26°, corresponding to the PET (100) plane similar to the previously published reports.<sup>[55–59]</sup> Ji et al. demonstrate that the diffraction peak position (i.e., 34.4°) is increased for higher seed layer thickness (over 500 and 1000 nm) deposited on glass substrates due to the internal compressive stress and lowering the seed layer thickness is not influencing that much.<sup>[60]</sup> Therefore, AZO seed layers show an improved crystalline quality for thicker films, which has a direct consequence on the properties of the subsequent ZnO NWs growth. Noticeably, ZnO NWs/seed layer AZO<sub>250</sub>-based films indicate the highest (002) peak intensity compared to the two other seed layer thicknesses (i.e., AZO<sub>100</sub> and AZO<sub>200</sub>, see Figure 2a–c and Figure S1, Supporting Information). The crystallinity of the ZnO NWs is, in fact, enhanced. Our investigations show a tiny shift of the (002) diffraction peak (see Figure S1, Supporting Information), in agreement with a previous report.<sup>[60]</sup> In addition, no secondary phases related to aluminum are detected, proving that the prepared ZnO NWs film shows an excellent crystalline structure. Furthermore, the annealing of the PET-ITO<sub>60</sub>-AZO<sub>250</sub>-NW film at 100 °C shows similar structural behavior as nonannealed films (see

Figure 2d), especially in the fitted spectra (see Figure S2a,b, Supporting Information), the variation in the peak position (i.e., 0.016), full width at half maximum (i.e., 0.004), and intensities (i.e., 3.35) are not shifting much compared to the PET-ITO<sub>60</sub>-AZO<sub>250</sub>-NW\_WOA film, which indicates that there is no need for annealing to enhance the crystallinity of the NWs. Therefore, the structural results demonstrate that seed layer AZO<sub>250</sub> is more promising for the growth of ZnO NWs.

### 3.2. Optical Analysis

The transmittance spectra of ZnO NWs grown on flexible substrates with different AZO seed layer thicknesses as a function of the wavelength in the range from 300 to 800 nm are shown in Figure 3a–c. The fluctuations in the spectral shape are attributed to an interference phenomenon between the top and bottom surfaces.<sup>[61]</sup> It is clear from Figure 3a that the ZnO NWs containing films (PET-ITO<sub>60</sub>-AZO<sub>100</sub>-NW, PET-ITO<sub>60</sub>-AZO<sub>200</sub>-NW, and PET-ITO<sub>60</sub>-AZO<sub>250</sub>-NW) show reduced transmittance compared to the films without NWs (PET-ITO<sub>60</sub>-AZO<sub>100</sub>, PET-ITO<sub>60</sub>-AZO<sub>200</sub>, and PET-ITO<sub>60</sub>-AZO<sub>250</sub>). Also, the film based on lower seed layer thickness (i.e., AZO<sub>100</sub>) with and without NWs demonstrates higher transmittance than the other two samples (i.e., AZO<sub>200</sub> and AZO<sub>250</sub>). The other substrates, that is to say PET-ITO<sub>200</sub>-AZO<sub>100</sub>-NW, PET-ITO<sub>200</sub>-AZO<sub>200</sub>-NW, and PET-ITO<sub>200</sub>-AZO<sub>250</sub>-NW, as well as PET\_AZO<sub>100</sub>-NW, PET\_AZO<sub>200</sub>-NW, and PET\_AZO<sub>250</sub>-NW films, also show a similar trend (see Figure 3b,c). All flexible substrates with ZnO NWs and seed layer AZO<sub>200</sub> or AZO<sub>250</sub> almost display similar transmittance. Rezaie et al. explain that the appropriate AZO layer thickness offers better transmittance due to the reduction of light scattering at grain boundaries.<sup>[37]</sup> In addition, the annealing (at 100 °C) does not influence the transmittance behavior (see Figure 3d), which is similar to structural data, confirming that the annealing process is not required.

The absorbance curves of ZnO NWs grown on different seed layer thicknesses (AZO<sub>100</sub>, AZO<sub>200</sub>, and AZO<sub>250</sub>) using various flexible substrates (PET, PET-ITO<sub>60</sub>, and PET-ITO<sub>200</sub>) are shown in Figure S3a–c, Supporting Information. The bandgap of the films was determined using the following formula  $(ah\nu)^2 = A(h\nu - E_g)^2$ ,<sup>[62]</sup> where the values are extrapolated from  $(ah\nu)^2$  versus energy (eV) plot. The calculated bandgaps of the PET-ITO<sub>60</sub>-AZO<sub>x</sub>-NW, PET-ITO<sub>200</sub>-AZO<sub>x</sub>-NW, and PET\_AZO<sub>x</sub>-NW films (where  $x = 100, 200, \text{ and } 250$ ) are displayed in Figure S3a'–c', Supporting Information, and the obtained bandgap ranges (i.e., 3.24–3.27 eV) are consistent with a previous report.<sup>[63]</sup> It is clear that the slight variations in the bandgaps correspond to the different seed layer thicknesses, such as AZO<sub>100</sub>, AZO<sub>200</sub>, and AZO<sub>250</sub> (see Figure S3a'–c', Supporting Information). In addition, the difference in the bandgaps for different substrates-based films (i.e., PET, PET-ITO<sub>60</sub>, and PET-ITO<sub>200</sub>) may be correlated to the ITO layer thicknesses; for example, 130 nm for 60 Ω sq<sup>-1</sup> ITO substrates compared to 40 nm with 200 Ω sq<sup>-1</sup> ITO substrates. Based on Figure 3 and Figure S3, Supporting Information, the difference between AZO<sub>200</sub> and AZO<sub>250</sub> is limited, and according to the XRD data, AZO<sub>250</sub> films offer good crystallinity. Therefore, the choice of ZnO NWs growth on AZO<sub>250</sub> is beneficial for our further studies.



**Figure 2.** XRD spectra of a) PET-ITO<sub>60</sub>-AZO<sub>x</sub>, b) PET-ITO<sub>200</sub>-AZO<sub>x</sub>, and c) PET-AZO<sub>x</sub> films with and without NW (where  $x = 100, 200,$  and  $250$ ). d) XRD spectra of PET-ITO<sub>60</sub>-AZO<sub>250</sub>-NW-WA and PET-ITO<sub>60</sub>-AZO<sub>250</sub>-NW-WOA films.

### 3.3. Morphological and Topographical Analysis

The surface morphology of the ZnO NWs grown on flexible substrates with different AZO seed layer thicknesses (AZO<sub>100</sub>, AZO<sub>200</sub>, and AZO<sub>250</sub>) is shown in Figure 4a–i. A summary of the ZnO NWs average diameter and density of PET-ITO<sub>60</sub>-AZO<sub>x</sub>-NW, PET-ITO<sub>200</sub>-AZO<sub>x</sub>-NW, and PET-AZO<sub>x</sub>-NW films (where  $x = 100, 200,$  and  $250$ ) is displayed in Table 2. The higher ZnO NWs density may be due to the NWs smaller diameter, and Figure 4 and Table 2 show that the AZO seed layer thickness strongly influences the ZnO NWs growth. For example, on the lower thickness seed layer (i.e., AZO<sub>100</sub>), thinner ZnO NWs can be observed compared to the two other AZO seed layer thicknesses (i.e., AZO<sub>200</sub> and AZO<sub>250</sub>, see Figure 4 and Table 2). Also, our previous report explains that the ZnO NWs grown over very thin seed layers show a tendency to interconnect due to high density and alignment.<sup>[46]</sup> The lower seed layer thicknesses (i.e., AZO<sub>100</sub> and AZO<sub>200</sub>) lead to an increase of nucleation sites on the surface of the AZO seed layer, resulting in higher ZnO NWs densities (see Table 2) compared to AZO<sub>250</sub>, and in agreement to the literature.<sup>[46,51,60]</sup> Figure 4d,g shows that the ZnO NWs are

highly closely packed due to NWs possibly being attached to one another, as previously reported by Song et al.<sup>[64]</sup> Furthermore, Ji et al. explain that poorly aligned ZnO NWs growth happens when the seed layer thickness is low and with poor crystal characteristics. On the contrary, thicker seed layers with good crystalline structure offer well-aligned ZnO NWs growth.<sup>[60]</sup> More importantly, measuring ZnO NWs length is challenging for these kinds of orientations (i.e., because the higher and lower NWs are randomly noticed in Figure 4). In addition, Figure S4a,b, Supporting Information shows the SEM images of PET-ITO<sub>60</sub>-AZO<sub>250</sub>-NW-WA and PET-ITO<sub>60</sub>-AZO<sub>250</sub>-NW-WOA films. The corresponding NWs avg. diameter and NWs density values are summarized in Table S1, Supporting Information, and the difference between the obtained values is limited, similar to XRD and transmittance data. We confirm once again that annealing (at 100 °C) is not essential to produce high-quality samples for the photovoltaic application.

The AFM images of PET-ITO<sub>60</sub>-AZO<sub>250</sub>-NW, PET-IT<sub>200</sub>-AZO<sub>250</sub>-NW, and PET-AZO<sub>250</sub>-NW films are shown in Figure S5a–c, Supporting Information. These images also confirm several longer (i.e., height) ZnO NWs grown on flexible

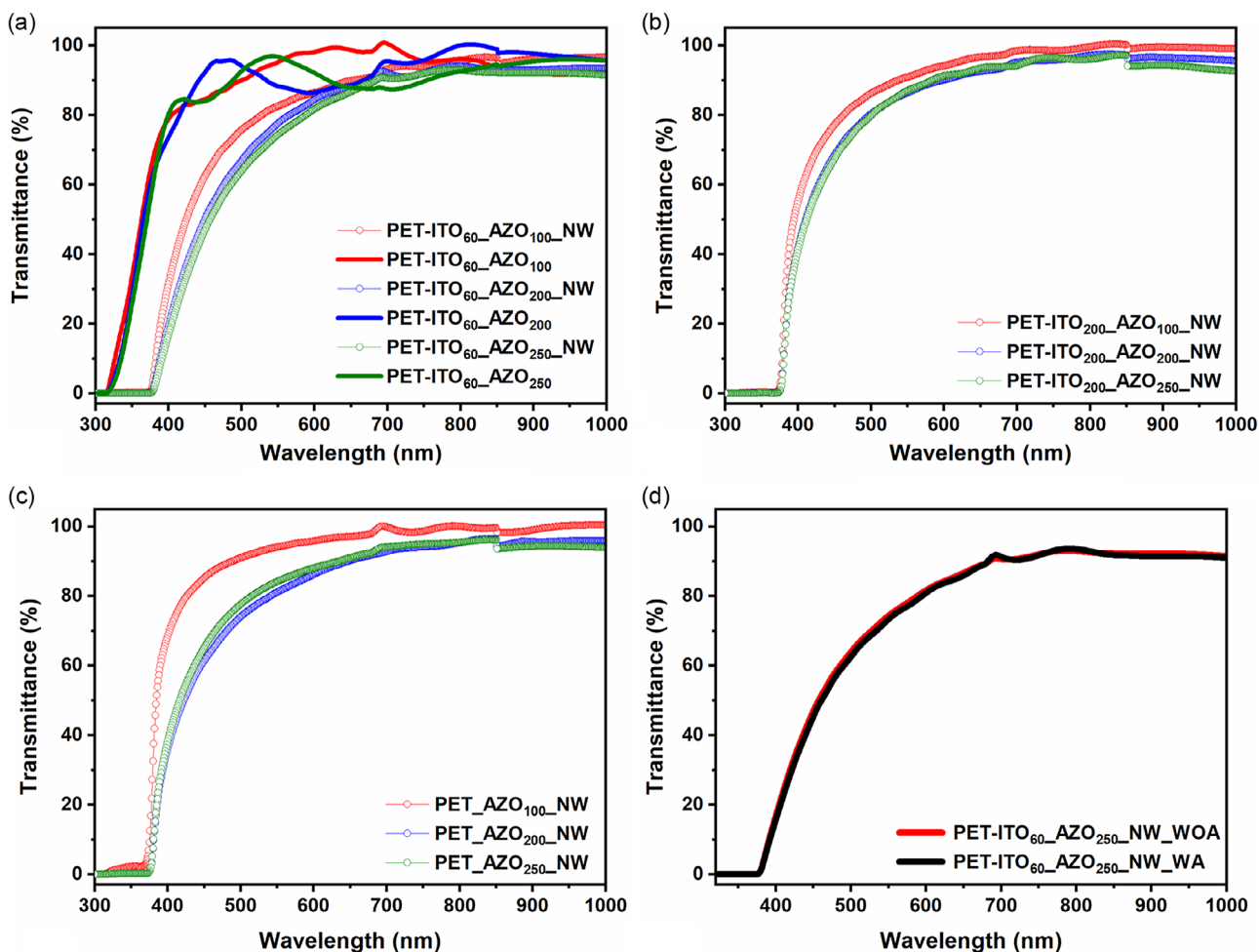


**Figure 3.** The transmittance spectra of a) PET-ITO<sub>60</sub>-AZO<sub>x</sub> films with and without NW, b) PET-ITO<sub>200</sub>-AZO<sub>x</sub>-NW, and c) PET-AZO<sub>x</sub>-NW films (where  $x = 100, 200,$  and  $250$ ). d) The transmittance spectra of PET-ITO<sub>60</sub>-AZO<sub>250</sub>-NW-WA and PET-ITO<sub>60</sub>-AZO<sub>250</sub>-NW-WOA films.

substrates with a thicker seed layer AZO<sub>250</sub> and a summary of the average roughness of PET-ITO<sub>60</sub>-AZO<sub>250</sub>-NW, PET-ITO<sub>200</sub>-AZO<sub>250</sub>-NW, and PET-AZO<sub>250</sub>-NW films is displayed in Table S2, Supporting Information. Noticeably, the roughness of the ZnO NWs films shows higher values on PET-ITO<sub>60</sub>-AZO<sub>250</sub>-NW and PET-AZO<sub>250</sub>-NW films than on PET-ITO<sub>200</sub>-AZO<sub>250</sub>-NW films (see Table S2, Supporting Information).

### 3.4. Flexible PSCs

According to the structural, optical, morphological, and topographical results, thick seed layer films (i.e., PET-ITO<sub>60</sub>-AZO<sub>250</sub>-NW, PET-IT<sub>200</sub>-AZO<sub>250</sub>-NW, and PET-AZO<sub>250</sub>-NW films) are chosen for fabricating FPSCs. Besides, as mentioned earlier, the spin-coating deposition technique, especially the anti-solvent treatment on the flexible substrates, affects the layer uniformity (see Figure S6a, Supporting Information). It is well known that, after depositing the perovskite layer, the annealing treatment at 100 °C on the hot plate is necessary to obtain a highly converted perovskite crystalline phase (black-colored  $\alpha$ -phase). However, in our case, we noticed the rapid appearance of a

yellow-colored phase, attributed to the optically inactive  $\delta$ -phase of the perovskite while annealing the perovskite-deposited PET-ITO<sub>60</sub>-AZO<sub>250</sub>-NW, PET-IT<sub>200</sub>-AZO<sub>250</sub>-NW, and PET-AZO<sub>250</sub>-NW films (see Figure S6b, Supporting Information). To resolve these issues, we pasted the ZnO NWs that grew flexible substrates on the same size glass substrate (see Figure 1b) to keep them flat during spin-coating. Initially, using all the selected PET-ITO<sub>60</sub>-AZO<sub>250</sub>-NW, PET-IT<sub>200</sub>-AZO<sub>250</sub>-NW, and PET-AZO<sub>250</sub>-NW films, the flexible PSCs are fabricated by adopting our previous rigid device conditions<sup>[2,47,48]</sup> and the corresponding photographs of the fabricated FPSCs are displayed in Figure S6c, Supporting Information. Unfortunately, none of the FPSCs showed any photovoltaic performance. Later, instead of testing all the films, we use the PET-ITO<sub>60</sub>-AZO<sub>250</sub>-NW film to fabricate the FPSC to get more information on the nonoptimized device.

The current density–voltage ( $J$ - $V$ ) characteristic of the nonoptimized PET-ITO<sub>60</sub>-AZO<sub>250</sub>-NW-WOA film-based FPSCs is shown in Figure 5a. Importantly, different spinning speeds (i.e., 1000, 1500, 2000, 2500, 3000, and 4000 rpm) were employed for the perovskite layer deposition to vary the layer thickness and to investigate the impact of ZnO NWs/perovskite interface. The

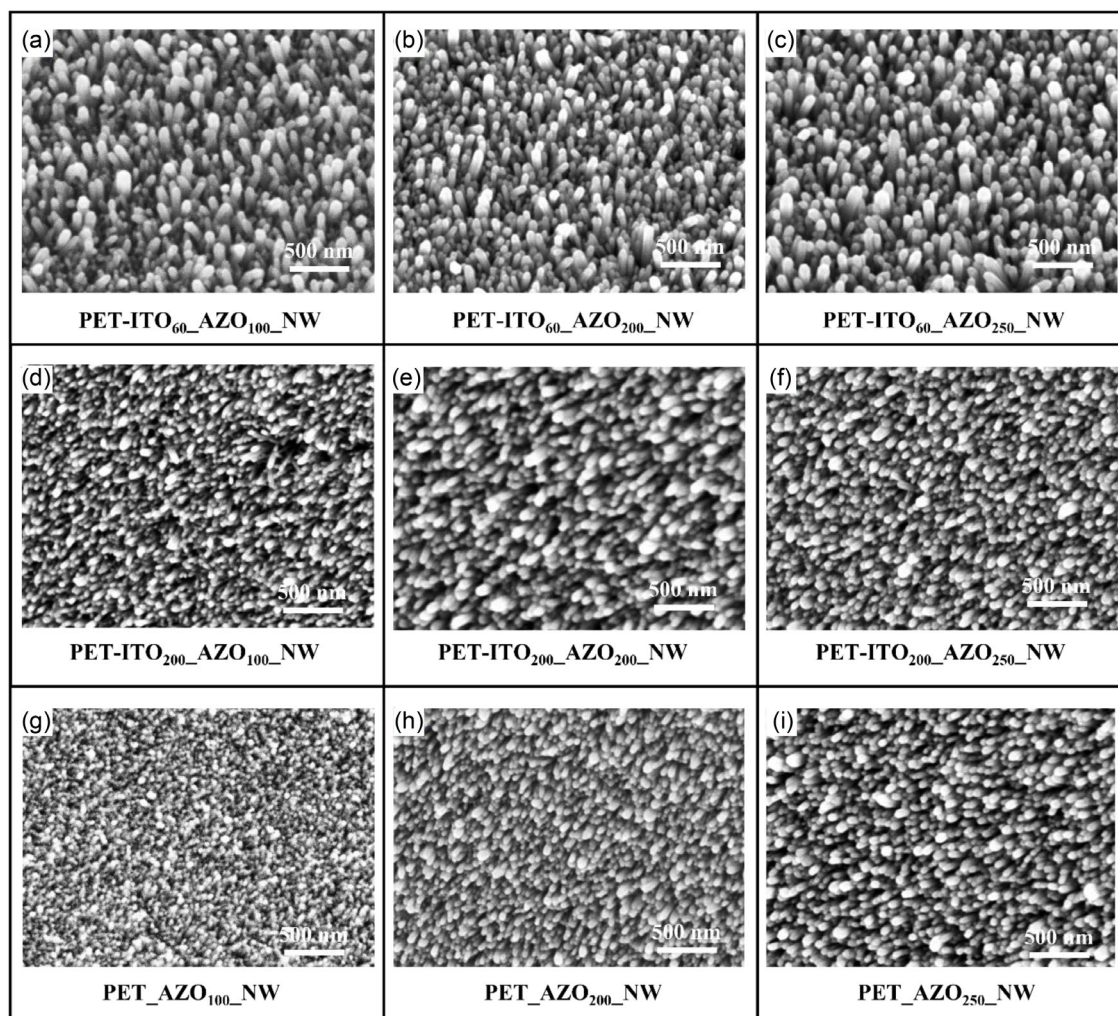


**Figure 4.** SEM images of a–c) PET-ITO<sub>60</sub>-AZO<sub>x</sub>-NW, d–f) PET-ITO<sub>200</sub>-AZO<sub>x</sub>-NW, and g–i) PET-AZO<sub>x</sub>-NW films (where  $x = 100, 200,$  and  $250$ ).

**Table 2.** Summary of the NWs average diameter and NWs density of PET-ITO<sub>60</sub>-AZO<sub>x</sub>-NW, PET-ITO<sub>200</sub>-AZO<sub>x</sub>-NW, and PET-AZO<sub>x</sub>-NW films, where  $x = 100, 200,$  and  $250$ .

Samples	Diameter [nm]	Density [NW $\mu\text{m}^{-2}$ ]
PET-ITO <sub>60</sub> -AZO <sub>100</sub> -NW	73	41
PET-ITO <sub>60</sub> -AZO <sub>200</sub> -NW	88	75
PET-ITO <sub>60</sub> -AZO <sub>250</sub> -NW	95	44
PET-ITO <sub>200</sub> -AZO <sub>100</sub> -NW	73	110
PET-ITO <sub>200</sub> -AZO <sub>200</sub> -NW	95	64
PET-ITO <sub>200</sub> -AZO <sub>250</sub> -NW	78	96
PET-AZO <sub>100</sub> -NW	51	135
PET-AZO <sub>200</sub> -NW	70	91
PET-AZO <sub>250</sub> -NW	84	83

obtained  $J-V$  plot shows that our preliminary FPSC does not provide a decent  $J-V$  curve and considerable efficiency ( $\approx 0.01\%$ ). Therefore, the cross-sectional SEM images were used to

determine the issue of the nonworking devices, more particularly to understand deeper the role of the ZnO NWs/perovskite interface. It is clear from Figure 5b that the perovskite solution did not infiltrate well inside the ZnO NWs gap. Moreover, the longer ZnO NWs are in direct contact with the HTL, which creates direct current leakages in the SCs. Also, the cross-sectional SEM image of FPSC without HTL and Au is displayed in Figure 5c. It evidently shows that the perovskite layer thickness is not thick enough, which is the primary reason for the ZnO NWs penetration toward the HTL. Indeed, the cross-sectional SEM images of Figure 5d,e clearly show that there is no direct contact between ZnO NWs and HTL. Therefore, it is clear that appropriate perovskite layer thickness is crucial to avoid direct contact between ZnO NWs and HTL. However, an infiltration issue is still noticed between the perovskite and ZnO NWs interface. In that consideration, we also tried the following two-step strategies for perovskite deposition<sup>[65]</sup> to compare the perovskite/NWs interface behavior.

In this case, the perovskite layer is deposited using a two-step process without antisolvent treatment, and the fabrication steps

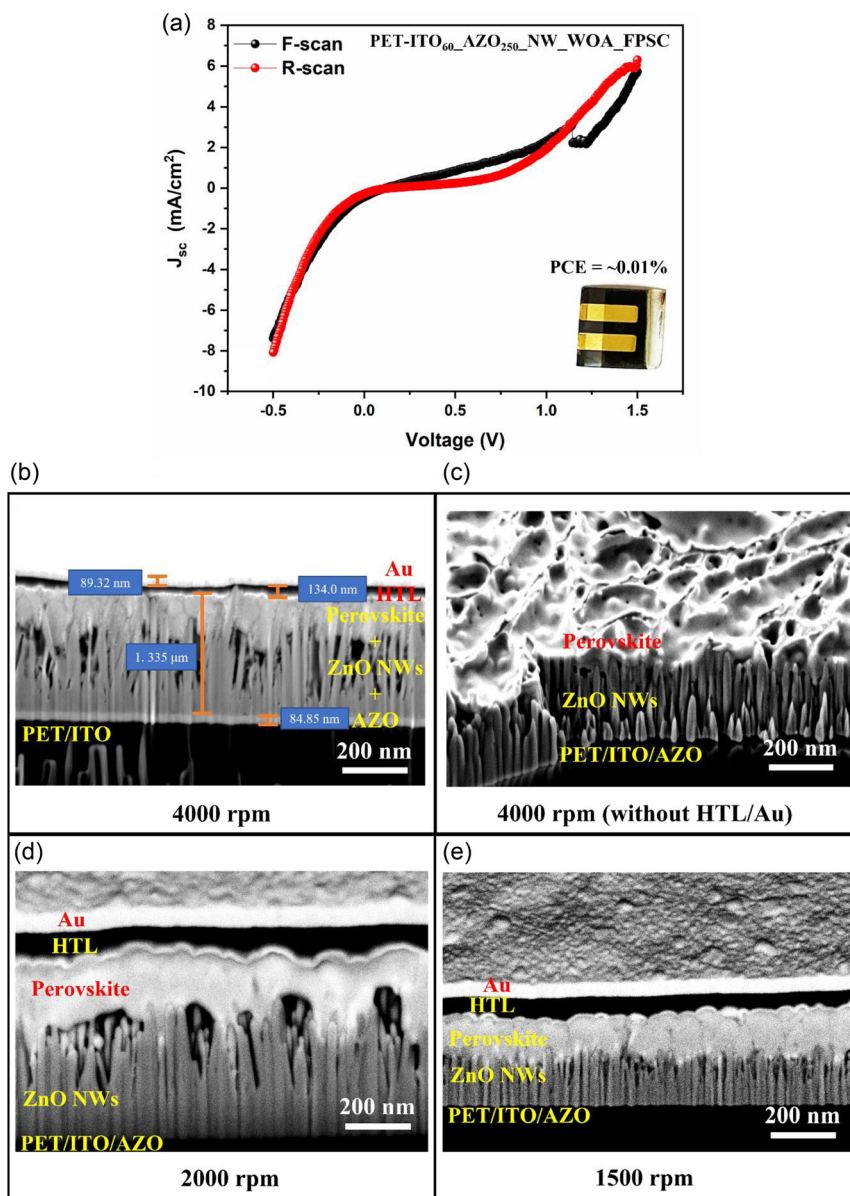


**Figure 5.** a)  $J$ - $V$  characteristics of fabricated PET-ITO<sub>60</sub>-AZO<sub>250</sub>-NW-WOA\_FPSC (inset: normal photograph). Cross-sectional SEM images of PET-ITO<sub>60</sub>-AZO<sub>250</sub>-NW-WOA\_FPSC with different absorber spinning speeds: b) 4000 rpm, c) 4000 rpm without HTL/Au, d) 2000 rpm, and e) 1500 rpm, respectively.

are shown in Figure S7a–f, Supporting Information. It slightly differs from the one-step deposition procedure; the precursor's solutions are prepared separately, such as CsI, PbI<sub>2</sub>, and PbBr<sub>2</sub> with DMF + DMSO mixture at 70 °C (i.e., solution 1) and FAI with IPA at room temperature (i.e., solution 2). Solution 1 is deposited on the PET/ITO/AZO/ZnO NW film and immediately annealed at 70 °C. Later, solution 2 is deposited and annealed at 100 °C before etching the perovskite layer. However, the fabricated FPSCs using PET-ITO<sub>60</sub>-AZO<sub>250</sub>-NW-WOA films are rapidly degrading under ambient air, as revealed through the yellow-colored  $\delta$ -perovskite phase (see Figure 6a) compared to the one-step process, and the corresponding SC cross-sectional

SEM image is shown in Figure 6b. Therefore, it is evident that despite suitable ZnO NW properties revealed in the first parts of this article, the fabrication protocol used for rigid devices is not suitable for flexible devices. Indeed, this study provides a solid reason for the nonworking devices. As a result, this study opens the way for device integration using dedicated protocols and methods.

Usually, in SCs, the charge carrier collection, separation, and recombination generally occur at the interfaces, mainly at ETL/absorber and absorber/HTL interfaces. Therefore, improving the perovskite/ZnO NWs interface in FPSCs is crucial to minimizing the interfacial energy barriers for charge carrier

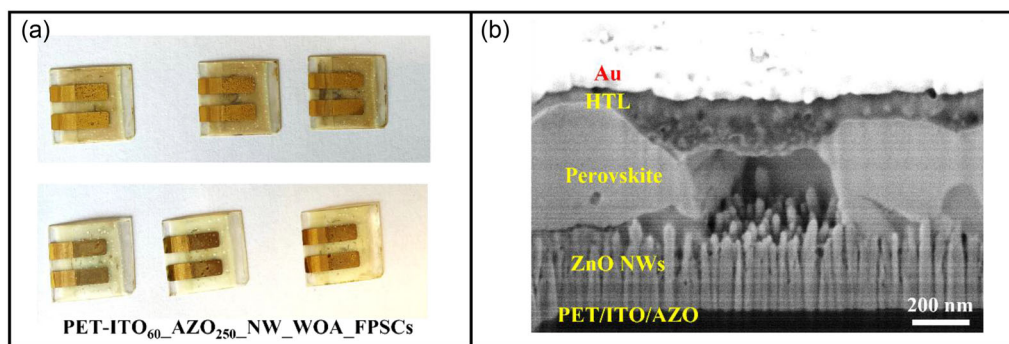


**Figure 6.** Fabricated FPSC using ITO<sub>60</sub>-AZO<sub>250</sub>-NW-WOA films: a) normal photographs and b) cross-sectional SEM image of perovskite layer deposited by a two-step process.

transport and suppressing recombinations, which enhances the SC performance. For example, cobalt-doped ZnO NWs film offers a higher transmittance than conventional NWs film, and the corresponding device offers better charge carrier transfer and reduced recombinations.<sup>[66]</sup> Also, modifying the ZnO NRs/perovskite interface by adding a ZnS interlayer in FPSCs alters the energy-level alignment and simultaneously improves the Zn–S–Pb coordination bond with perovskite, improving the charge carrier (i.e., electron) transport.<sup>[34]</sup> According to these reports, doping/interlayer/core–shell modification between ZnO NWs/perovskite interface provides a promising path toward stable and highly efficient FPSCs.

#### 4. Conclusion

The ZnO NWs have been successfully grown on AZO seed layer-coated flexible substrates (PET-ITO<sub>60</sub>-AZO<sub>100</sub>-NW, PET-ITO<sub>60</sub>-AZO<sub>200</sub>-NW and PET-ITO<sub>60</sub>-AZO<sub>250</sub>-NW, PET-ITO<sub>200</sub>-AZO<sub>100</sub>-NW, PET-ITO<sub>200</sub>-AZO<sub>200</sub>-NW, and PET-ITO<sub>200</sub>-AZO<sub>250</sub>-NW, as well as PET-AZO<sub>100</sub>-NW, PET-AZO<sub>200</sub>-NW, and PET-AZO<sub>250</sub>-NW). The structural analysis shows a higher (002) peak intensity for ZnO NWs on the thicker seed layer films (i.e., AZO<sub>250</sub>) than the other two films (i.e., AZO<sub>100</sub> and AZO<sub>200</sub>). Transmittance results confirm that in all three cases (PET, PET-ITO<sub>60</sub>, and PET-ITO<sub>200</sub>), the lower seed layer thickness films (i.e., AZO<sub>100</sub>) with and without NWs demonstrate higher transmittance than the thicker seed layer films (i.e., AZO<sub>200</sub> and AZO<sub>250</sub>). The morphological analysis proves that the AZO seed layer thickness on the different substrates (i.e., PET, PET-ITO<sub>60</sub>, and PET-ITO<sub>200</sub>) strongly impacts ZnO NWs growth. For example, considering the NWs diameter, the ZnO NWs on the lower thickness seed layer (i.e., AZO<sub>100</sub>) show thinner NWs compared to the other two AZO seed layer thicknesses. However, the NWs density values do not follow the tendency by means of displaying linear and nonlinear variations. The AFM images of PET-ITO<sub>60</sub>-AZO<sub>250</sub>-NW, PET-ITO<sub>200</sub>-AZO<sub>250</sub>-NW, and PET-AZO<sub>250</sub>-NW films also confirm that several shorter and longer ZnO NWs are randomly grown on flexible substrates. In addition, annealing the film at 100 °C (after ZnO NWs growth) shows similar structural (XRD), optical (transmittance and absorbance), and morphological (SEM) behavior as nonannealed films (the

difference is minimal), confirming that there is no need for annealing to improve the crystallinity of the NWs. A thicker seed layer (AZO<sub>250</sub>)-coated flexible substrates with ZnO NWs are chosen to fabricate the preliminary FPSCs. Noticeably, the fabricated preliminary FPSC SEM cross-sectional images mainly demonstrate the reasons for the nonworking device: 1) longer ZnO NWs in direct contact with HTL (Figure 5b) and 2) insufficient perovskite absorber thickness (Figure 5c–e). It is confirmed that besides the suitable ZnO NW properties, the fabricated preliminary devices did not demonstrate any decent performance while adopting a rigid device fabrication protocol. Therefore, systematic optimization, including dedicated protocols and methods, is essential to get working FPSCs. To conclude, the performance of PSC depends on all layers in the chosen device configuration, such as ETL, absorber, HTL, and bottom and top electrodes. Therefore, finding and resolving issues, like interface/surface or recombination issues, are essential to achieving higher SC PCE.

#### Supporting Information

Supporting Information is available from the Wiley Online Library or from the author.

#### Acknowledgements

The authors gratefully acknowledge the Regional Council Centre-Val de Loire, who supported the MASOFLEX project. This work has also received support under the CERTeM 5.0 Program, with the financial support of the Regional Council Centre-Val de Loire and Tours Val de Loire Metropolis (France). Similarly, this work was partially supported by the French National Research Agency (ANR-10-LABX-0074-01 Sigmalmim). K.S. and J.B. specifically acknowledge the PLATINOM technology platform (University of Limoges), which hosted all device fabrication and characterization steps. Also, M.B. (GREMAN, Tours) and S.R. (Xlim, Limoges) are acknowledged for their valuable support.

#### Conflict of Interest

The authors declare no conflict of interest.

## Author Contributions

**Karthick Sekar:** formal analysis (lead); investigation (lead); methodology (lead); writing—original draft (lead); writing—review and editing (lead). **Johann Bouclé:** formal analysis (equal); validation (equal); writing—review and editing (equal). **Raphaël Doineau:** formal analysis (supporting). **Souhir Azzaz:** formal analysis (supporting). **Bruno Schmaltz:** writing—review and editing (supporting). **Guylaine Poulin-Vittrant:** conceptualization (lead); formal analysis (equal); supervision (lead); writing—review and editing (lead).

## Data Availability Statement

The data that support the findings of this study are available in the supplementary material of this article.

## Keywords

flexible substrates, hydrothermal growths, perovskite solar cells, ZnO NWs

Received: June 6, 2024  
Revised: December 17, 2024  
Published online:

- [1] T. Slimani Tlemcani, C. Justeau, K. Nadaud, D. Alquier, G. Poulin-vittrant, *Nanomaterials* **2021**, *11*, 1433.
- [2] K. Sekar, R. Nakar, J. Bouclé, R. Doineau, K. Nadaud, B. Schmaltz, G. Poulin-Vittrant, *Nanomaterials* **2022**, *12*, 2093.
- [3] S. Rabhi, T. A. Hameed, S. Mayarambakam, M. Khalid Hossain, K. Sekar, *Heliyon* **2024**, *10*, e31138.
- [4] T. Voss, S. R. Waldvogel, *Mater. Sci. Semicond. Process.* **2017**, *69*, 52.
- [5] D. Vanmaekelbergh, L. K. Van Vugt, *Nanoscale* **2011**, *3*, 2783.
- [6] D. P. Neveling, T. S. Van Den Heever, W. J. Perold, L. M. T. Dicks, *Sens. Actuators, B* **2014**, *203*, 102.
- [7] N. Caicedo, R. Leturcq, J. P. Raskin, D. Flandre, D. Lenoble, *Sens. Actuators, B* **2019**, *297*, 126602.
- [8] C. Soci, A. Zhang, B. Xiang, S. A. Dayeh, D. P. R. Aplin, J. Park, X. Y. Bao, Y. H. Lo, D. Wang, *Nano Lett.* **2007**, *7*, 1003.
- [9] J. Wang, S. Lee, A. R. Bielski, K. A. Meyer, A. Dhyani, A. M. Ortiz-Ortiz, A. Tuteja, N. P. Dasgupta, *Adv. Mater. Interfaces* **2020**, *7*, 2000672.
- [10] C. M. Taylor, A. Ramirez-Canon, J. Wenk, D. Mattia, *J. Hazard. Mater.* **2019**, *378*, 120799.
- [11] Z. L. Wang, *J. Phys.:Condens. Matter* **2004**, *16*, 829.
- [12] Ü. Özgür, Y. I. Alivov, C. Liu, A. Teke, M. A. Reshchikov, S. Doğan, V. Avrutin, S. J. Cho, *J. Appl. Phys.* **2005**, *98*, 1.
- [13] L. E. Greene, B. D. Yuhas, M. Law, D. Zitoun, P. Yang, *Inorg. Chem.* **2006**, *45*, 7535.
- [14] A. Wibowo, M. A. Marsudi, M. I. Amal, M. B. Ananda, R. Stephanie, H. Ardy, L. J. Diguna, *RSC Adv.* **2020**, *10*, 42838.
- [15] A. S. Dahiya, S. Boubenia, G. Franzo, G. Poulin-Vittrant, S. Mirabella, D. Alquier, *Nanoscale Res. Lett.* **2018**, *13*, 249.
- [16] A. Galdámez-Martinez, G. Santana, F. Güell, P. R. Martínez-Alanis, A. Dutt, *Nanomaterials* **2020**, *10*, 857.
- [17] A. S. Dahiya, C. Opoku, D. Alquier, G. Poulin-Vittrant, F. Cayrel, O. Graton, L. P. T. Huu Hue, N. Camara, *Nanoscale Res. Lett.* **2014**, *9*, 1.
- [18] N. Faraji, C. Ulrich, N. Wolff, L. Kienle, R. Adelung, Y. K. Mishra, J. Seidel, *Adv. Electron. Mater.* **2016**, *2*, 1600138.
- [19] M. A. Susner, S. D. Carnevale, T. F. Kent, L. M. Gerber, P. J. Phillips, M. D. Sumption, R. C. Myers, *Phys. E* **2014**, *62*, 95.
- [20] I. Isakov, M. Panfilova, M. J. L. Sourribes, P. A. Warburton, *Phys. Status Solidi C* **2013**, *10*, 1308.
- [21] Z. Zheng, L. Gan, J. B. Zhang, F. Zhuge, T. Y. Zhai, *Adv. Sci.* **2017**, *4*, 1600316.
- [22] I. Z. Papp, A. Alegría, Z. Kónya, Á. Kukovecz, *Mater. Res. Bull.* **2022**, *149*, 111701.
- [23] A. Hamdi, A. Hamieh, M. Alamri, K. Dogheche, M. M. S. Mohan, R. Desfeux, D. Remiens, E. Dogheche, *Surf. Interfaces* **2022**, *31*, 102103.
- [24] P. Rong, S. Ren, Q. Yu, *Crit. Rev. Anal. Chem.* **2019**, *49*, 336.
- [25] Y. Hu, T. Niu, Y. Liu, Y. Zhou, Y. Xia, C. Ran, Z. Wu, L. Song, P. Müller-Buschbaum, Y. Chen, W. Huang, *ACS Energy Lett.* **2021**, *6*, 2917.
- [26] D. Yang, R. Yang, S. Priya, S. Liu, *Angew. Chem. Int. Ed.* **2019**, *58*, 4466.
- [27] Y. Lv, B. Cai, R. Yuan, Y. Wu, Q. Qiao, W. H. Zhang, *J. Energy Chem.* **2023**, *82*, 66.
- [28] A. R. A. Rashid, H. K. Tazri, *Nano Hybrids Compos.* **2021**, *31*, 25.
- [29] V. Consonni, J. Briscoe, E. Kärber, X. Li, T. Cossuet, *Nanotechnology* **2019**, *30*, 362001.
- [30] M. Xing, L. Wang, R. Wang, *Nanomaterials* **2022**, *12*, 114.
- [31] M. H. Kumar, N. Yantara, S. Dharani, M. Graetzel, P. P. Boix, N. Mathews, *Chem. Commun.* **2013**, *49*, 11089.
- [32] A. Dymshits, L. Iagher, L. Etgar, *Materials* **2016**, *9*, 60.
- [33] J. Sun, Q. Hua, R. Zhou, D. Li, W. Guo, X. Li, G. Hu, C. Shan, Q. Meng, L. Dong, C. Pan, Z. L. Wang, *ACS Nano* **2019**, *13*, 4507.
- [34] M. Fahim, I. Firdous, W. Zhang, W. A. Daoud, *Nano Energy* **2021**, *86*, 106127.
- [35] Y. Geng, K. Jeronimo, M. A. Bin Che Mahzan, P. Lomax, E. Mastropaolo, R. Cheung, *Nanoscale Adv.* **2020**, *2*, 2814.
- [36] K. Sekar, R. Doineau, S. Mayarambakam, B. Schmaltz, G. Poulin-Vittrant, *Heliyon* **2024**, *10*, e24706.
- [37] M. N. Rezaie, N. Manavizadeh, F. D. Nayeri, M. M. Bidgoli, E. Nadimi, F. A. Boroumand, *Ceram. Int.* **2018**, *44*, 4937.
- [38] C. Justeau, T. S. Tlemcani, G. Poulin-Vittrant, K. Nadaud, D. Alquier, *Materials* **2019**, *12*, 2511.
- [39] T. A. Nirmal Peiris, H. Alessa, J. S. Sagu, I. Ahmad Bhatti, P. Isherwood, K. G. Upul Wijayantha, *J. Nanopart. Res.* **2013**, *15*, 1.
- [40] F. Dehghan Nayeri, E. Asl Soleimani, *Exp. Tech.* **2014**, *38*, 13.
- [41] E. D. Matheson, Y. Qu, G. Kartopu, M. K. Etherington, G. Zoppi, V. Barrioz, N. S. Beattie, *J. Mater. Sci.: Mater. Electron.* **2023**, *34*, 1.
- [42] H. Ghosh, B. Sadeghimakki, S. Sivoththaman, *Mater. Res. Express* **2020**, *7*, 035013.
- [43] Q. C. Bui, V. Consonni, S. Boubenia, G. Gay, C. Perret, M. Zeghouane, S. Labau, C. Jiménez, H. Roussel, X. Mescot, G. Ardila, B. Salem, *ACS Appl. Nano Mater.* **2023**, *6*, 7436.
- [44] A. Serrano, A. Arana, A. Galdámez, A. Dutt, B. M. Monroy, F. Güell, G. Santana, *Vacuum* **2017**, *146*, 509.
- [45] W. S. Cheng, J. R. Lai, H. T. Hsueh, T. C. Cheng, *Sens. Mater.* **2023**, *35*, 1089.
- [46] T. S. Tlemcani, C. Justeau, K. Nadaud, G. Poulin-Vittrant, D. Alquier, *Chemodosensors* **2019**, *7*, 7.
- [47] S. Karthick, S. Velumani, J. Bouclé, *Sol. Energy* **2020**, *205*, 349.
- [48] S. Karthick, H. Hawashin, N. Parou, S. Vedraïne, S. Velumani, J. Bouclé, *Sol. Energy* **2021**, *218*, 226.
- [49] K. Sekar, R. Manisekaran, O. M. Nwakanma, M. Babudurai, *Adv. Energy Sustainability Res.* **2024**, *5*, 2400003.
- [50] B. Ikizler, S. M. Peker, *Thin Solid Films* **2014**, *558*, 149.
- [51] H. Ghayour, H. R. Rezaie, S. Mirdamadi, A. A. Nourbakhsh, *Vacuum* **2011**, *86*, 101.
- [52] Z. H. Azmi, S. N. Mohd Aris, S. Abubakar, S. Sagadevan, R. Siburian, S. Paiman, *Coatings* **2022**, *12*, 474.
- [53] Q. Liu, T. Yasui, K. Nagashima, T. Yanagida, M. Hara, M. Horiuchi, Z. Zhu, H. Takahashi, T. Shimada, A. Arima, Y. Baba, *J. Phys. Chem. C* **2020**, *124*, 20563.

- [54] N. Akin, S. Sebnem Cetin, M. Cakmak, T. Memmedli, S. Ozcelik, *J. Mater. Sci.: Mater. Electron.* **2013**, *24*, 5091.
- [55] S. G. Prasad, A. De, U. De, R. W. Berg, *Int. J. Spectrosc.* **2011**, *2011*, 810936.
- [56] Y. A. Stetsiv, M. M. Yatsyshyn, D. Nykypanchuk, S. A. Korniy, I. Saldan, O. V. Reshetnyak, T. J. Bednarchuk, *Polym. Bull.* **2020**, *78*, 6251.
- [57] Y. Zhang, Y. Jia, L. Hou, *RSC Adv.* **2018**, *8*, 31471.
- [58] J. A. Yabagi, M. H. Jameel, A. H. Jabbar, M. I. Kimpa, R. Qays Malik, S. P. Xin, N. Babakatcha, M. B. Ladan, M. Q. Hamzah, M. A. Agam, M. M. Hessien, G. A. M. Mersal, *RSC Adv.* **2022**, *12*, 32949.
- [59] S. Agrawal, N. Ingle, U. Maity, R. V. Jasra, P. Munshi, *ACS Omega* **2018**, *3*, 6692.
- [60] L. W. Ji, S. M. Peng, J. S. Wu, W. S. Shih, C. Z. Wu, I. T. Tang, *J. Phys. Chem. Solids* **2009**, *70*, 1359.
- [61] J. Zhang, W. Que, *Sol. Energy Mater. Sol. Cells* **2010**, *94*, 2181.
- [62] X. Peng, W. Wang, Y. Zeng, X. Pan, Z. Ye, Y. Zeng, *RSC Adv.* **2018**, *8*, 33174.
- [63] J. O. Hwang, D. H. Lee, J. Y. Kim, T. H. Han, B. H. Kim, M. Park, K. No, S. O. Kim, *J. Mater. Chem.* **2011**, *21*, 3432.
- [64] J. Song, S. Lim, *J. Phys. Chem. C* **2006**, *111*, 596.
- [65] Y. Han, H. Xie, E. L. Lim, D. Bi, *Sol. RRL* **2022**, *6*, 2101007.
- [66] F. Bouhjar, L. Derbali, B. Marí, *Nano Res.* **2020**, *13*, 2546.